APPLICATION OF RIGID BODIES-SPRING MODEL TO PRECAST STRUCTURE REINFORCED WITH STEEL FIBER

Hamadi ZARDOUM*, Yasuo KAJIKAWA**, Michihiro TOMIDA*** and Hiroshi MASUYA****

*Doctoral student, Graduate School of Natural Science and Technology, Kanazawa University, Kodatsuno 2-40-20, Kanazawa 920-8667

**Professor, Graduate School of Natural Science and Technology, Kanazawa University, Kodatsuno 2-40-20, Kanazawa 920-8667

*** Associate Professor, Dept. of Civil Eng., Ishikawa National College of Technology, Tsubata, Ishikawa

**** Associate Professor, Dept. of Civil Eng., Kanazawa University, Kodatsuno 2-40-20, Kanazawa 920-8667

This paper presents an experimental and analytical study on the behavior of a precast prestressed concrete structure reinforced with steel fiber reinforced concrete (herein after written SFRC) in the joint.

The effect of the SFRC on the crack pattern, failure mode and the flexural behavior of the structure were investigated. The analysis method used in this study is the Rigid Bodies-Spring Model [1] (herein after written RBSM). The prestressing steel bar (herein after written pr-bar) was introduced, into the RBSM, as the beam element [2), 3)], however The SFRC was considered as a special material taking in the phenomenon of tension stiffening [4)].

It was confirmed that the SFRC could be a very suitable material to reinforce the joint of a precast structure. On the other hand, the RBSM is an effective model for analyzing the flexural behavior of any kind of structure.

Key Words: Precast Structure, SFRC, RBSM

1. INTRODUCTION

Precast concrete structure has been widely used in the field of construction for a long time and it is still used up to nowadays. In this type of structure, it is remarkable that the weakest point is the joint zone, where the failure occurs often. On the other hand, it is well known that the use of fibers to concrete controls the appearance and the development of cracking and consequently increases durability of a structure. In the last few decades, there has been widely extensive development in the SFRC technology [5), 6)]. However, the use of this material in practical projects remains very rare because of the high cost of the fiber. Therefore, we propose the use of partial SFRC precast structures, so the SFRC was used in the joint zone to reinforce the structure and to limit the propagation of the cracks. In addition, this idea can reduce the cost of the structure.

In this study, there are two main objectives. The first one was to investigate experimentally the effect of the steel fiber on the crack pattern, failure mode and the flexural behavior of a precast prestressed concrete structure. The second was to introduce the SFRC as a special material taking in the phenomenon of tension stiffening into the RBSM method to analyze the precast structures reinforced with SFRC in the joint.

2. EXPERIMENTAL PROGRAM

2.1. Test Specimens

The experiments were done in a precast beam made of three rectangular reinforced concrete elements, tightened using a prestressing steel bar (pr-bar). The design dimensions and the reinforcement details of the specimen are shown in figure 1. To investigate the effect of the steel fiber on the behavior and failure load of the structure, a SFRC was used in the end side of element A, and both end sides of element B. In order to respect the design details, the specimens were cast in a vertical wood molds. First the plain concrete was cast and then, before the hardening of the plain concrete, the end side was cast with concrete mixed with steel fiber.

The experiments were divided into two cases depending on the fiber mixture rate, 0% in case 1 and 2% in case 2. The prestressing force in the two cases was 55 kN, with an eccentricity of 2.5 cm to the lower side.

2.2. Test Setup

Loading method and measured items are shown in figure 2. Taking the span length of 280 cm long as a simple support beam, two symmetrical loading points was carried out. The load was increased monotonously by the load control method until the beam reached final failure.

The deflections were measured at three points of the beam using displacement meters. The compressive and tensile strains, respectively in the upper and lower edge of the beam and the strain of the prestressing steel bar were measured using electric resistance strain gauges. The opening of the joint was measured using arch displacement meters and the loading force using a load cell.

2.3. Material Characteristics

The mechanical properties of the materials used in the specimens are summarized in table 1 and the characteristics of the steel fiber are given in table 2.

Figure 3 shows the uniaxial Stress-Strain relationship of the plain concrete presented with the dashed line. In this analysis, the relationship is approximated according to the plane line.

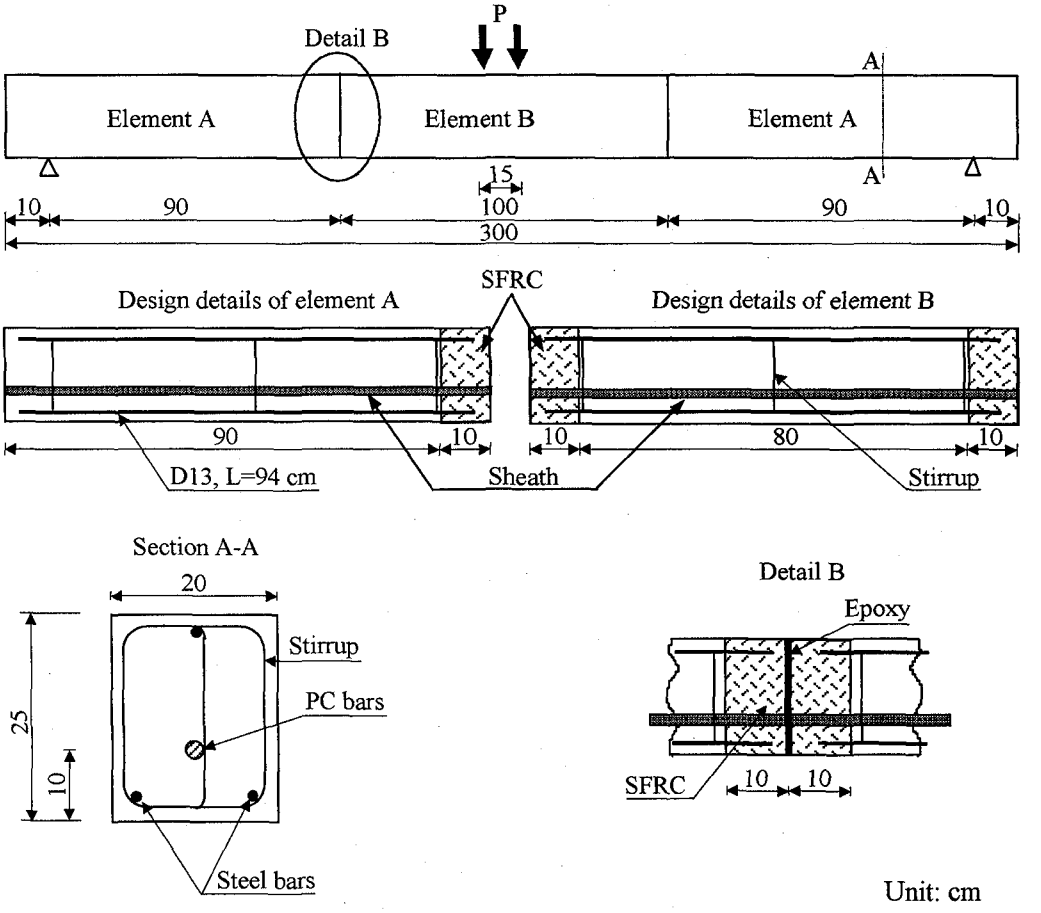

Figure 1 Layout and Design Details of Specimen

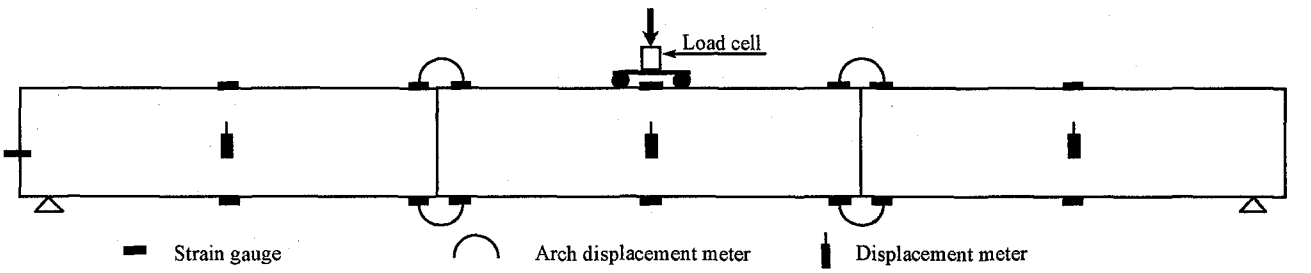

Figure 2 Loading Method and Measured Items

Table 1 Materials Characteristics

	Compressive Strength	Tensile Strength	Young's Modulus
Plain Concrete	48 MPa	3.0 MPa	31 GPa
SFRC 2%	48 MPa	6.2 MPa	37 GPa
	Yield Stress	Young's Modulus	
Steel Bar	300 MPa	210 GPa	
Pr-Bar	1030 MPa	207 GPa	

Table 2 Details of Steel Fiber

Length (mm)	50
Surface (mm)	0.60x1.00
Area (mm^2)	0.60
Aspect Ratio	57
Weight (mg)	236

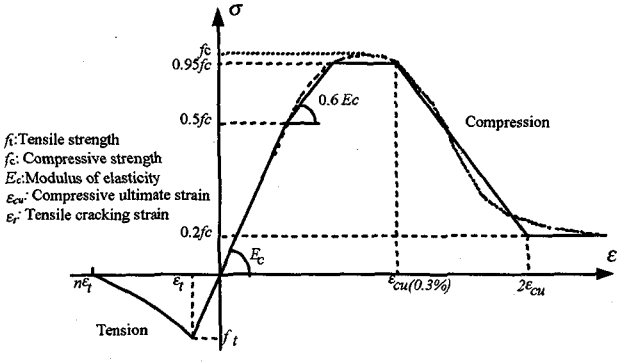

Figure 3 Stress-Strain Relationship for Plain Concrete

3. ANALYSIS

3.1. Brief Description of Two Dimensional RBSM [1), 7)]

This method considers two rigid triangular elements as shown in figure 4. Of course, an arbitrary polygon can be used instead of a triangular element. These elements are assumed to be in equilibrium with external loads and reaction forces of spring system, which is distributed over the contact surface of two adjacent bodies.

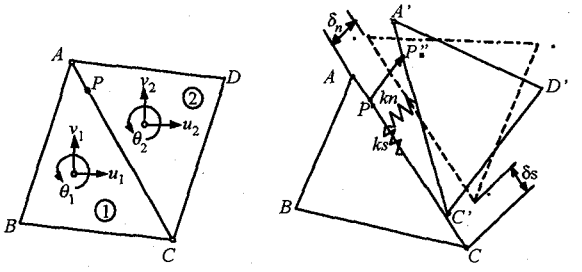

Figure 4 Rigid Triangular Elements

The rigid displacement field is assumed in each element in terms of the displacement (u, v, θ) of the centroid as shown in figure 4. More precisely, horizontal and vertical displacements U, V at the arbitrary point P (x, y) can be given by the following equations:

$$\boldsymbol{U} = \boldsymbol{Q}.\boldsymbol{u_i} \tag{1}$$

$$\boldsymbol{U} = \{U_I, V_I, U_{II}, V_{II}\}^T$$

$$\boldsymbol{u_i} = \{u_1, v_1, \theta_1, u_2, v_2, \theta_2\}^T$$

$$\boldsymbol{Q} = \begin{bmatrix} 1 & 0 & -(y-y_1) & 0 & 0 & 0 \\ 0 & 1 & (x-x_1) & 0 & 0 & 0 \\ 0 & 0 & 0 & 1 & 0 & -(y-y_2) \\ 0 & 0 & 0 & 0 & 1 & (x-x_2) \end{bmatrix}$$

Where subscript I, II or 1, 2 indicate element number ① or ②, respectively. (x_1, y_1) and (x_2, y_2) are the coordinate values of the centroid for each element.

The relation of the displacement between the global coordinate system and the local coordinate system along the side $\overline{CA}$ of the triangular element is derived by the following equation:

$$\overline{\boldsymbol{U}} = \boldsymbol{R}.\boldsymbol{U} \tag{2}$$

$$\overline{\boldsymbol{U}} = \{\overline{U}_I, \overline{V}_I, \overline{U}_{II}, \overline{V}_{II}\}^T$$

$$\boldsymbol{R} = \begin{bmatrix} l_1 & m_1 & 0 & 0 \\ l_2 & m_2 & 0 & 0 \\ 0 & 0 & l_1 & m_1 \\ 0 & 0 & l_2 & m_2 \end{bmatrix} \quad \begin{aligned} l_1 &= \cos(\bar{x},x) = y_{AC}/l_{CA} \\ l_2 &= \cos(\bar{x},y) = x_{AC}/l_{CA} \\ m_1 &= \cos(\bar{y},x) = x_{CA}/l_{CA} \\ m_2 &= \cos(\bar{y},y) = y_{AC}/l_{CA} \end{aligned}$$

Where l_{CA} is the length of side $\overline{CA}$, $x_{ij}=x_i-x_j$, the superscript (-) indicates the local coordinate system and R is a coordinate transformation matrix. Using these displacements $\overline{U}$, $\overline{V}$ with the local coordinate system, the relative displacement vector δ of the point P can be derived as follows:

$$\boldsymbol{\delta} = \boldsymbol{M}.\overline{\boldsymbol{U}} \tag{3}$$

$$\boldsymbol{\delta} = \{\delta_n, \delta_S\}^T \qquad \boldsymbol{M} = \begin{bmatrix} -1 & 0 & 1 & 0 \\ 0 & -1 & 0 & 1 \end{bmatrix}$$

Therefore, substituting eq.(1) and eq.(2) into eq.(3), the following relation with the rigid displacement field is easily obtained:

$$\boldsymbol{\delta} = \boldsymbol{M}.\boldsymbol{R}.\boldsymbol{Q}.\boldsymbol{u_i} = \boldsymbol{B}.\boldsymbol{u_i} \tag{4}$$

The spring constants k_n and k_s which resist normal and tangential forces respectively on the contact surface between element I and element II can be determined systematically, by using the finite difference equation for strain components, as follows:

$$\varepsilon_n = \frac{\delta_n}{h_1+h_2} = \frac{\delta_n}{h}$$
$$\gamma_s = \frac{\delta_s}{h_1+h_2} = \frac{\delta_s}{h} \qquad (5a, 5b)$$

Where $h=h_1+h_2$ is the projected length of a vector connecting centroids along the line perpendicular to $\overline{CA}$, as shown in figure 5.

On the contact surface $\overline{CA}$ shown in figure 4, the normal and tangential stresses σ_n, τ_s are assumed to satisfy the following equations:

$$\sigma_n = \frac{(1-\nu)E}{(1-2\nu)(1+\nu)}\varepsilon_n$$
$$\tau_s = \frac{E}{(1+\nu)}\gamma_s \qquad (6a, 6b)$$

Where ν is the Poisson's ratio and E is the Young's modulus.

Substituting eq.(5a, 5b) into eq.(6a, 6b), the following relations can be obtained:

$$\sigma_n = \frac{(1-\nu)E}{(1-2\nu)(1+\nu)}\frac{\delta_n}{h}$$
$$\tau_s = \frac{E}{(1+\nu)}\frac{\delta_s}{h} \qquad (7a, 7b)$$

On the other hand, from the definition of the spring constants, the following relations are obtained:

$$\sigma_n = k_n.\delta_n$$
$$\tau_s = k_s.\delta_s \qquad (8a, 8b)$$

Therefore, comparing eq.(7a, 7b) and eq.(8a, 8b), expressions for k_n and k_s can be derived as follows:

$$k_n = \frac{(1-\nu)E}{(1-2\nu)(1+\nu)h}$$
$$k_s = \frac{E}{(1+\nu)h} \qquad (9a, 9b)$$

From eq.(9) the stress-relative displacement relation is derived by the following matrix equation:

$$\boldsymbol{\sigma} = \boldsymbol{D}.\boldsymbol{\delta} \qquad (10)$$

$$\boldsymbol{\sigma} = \{\sigma_n, \tau_s\}^T \qquad \boldsymbol{D} = \begin{bmatrix} k_n & 0 \\ 0 & k_s \end{bmatrix}$$
$$\boldsymbol{\delta} = \{\delta_n, \delta_s\}^T$$

Based on the above preliminaries, the strain energy V stored in the spring system on $\overline{CA}$ can be obtained as the following matrix equations:

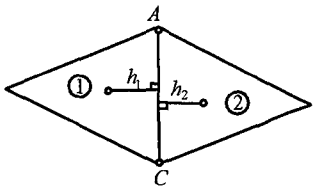

Figure 5 Definition of the Projected Length

$$V = \frac{t}{2}\int_{lCA} \boldsymbol{\delta}^T.\boldsymbol{D}.\boldsymbol{\delta}.ds = \frac{t}{2}u_i^T \int_{lCA}\left(\boldsymbol{B}^T.\boldsymbol{D}.\boldsymbol{B}\right)ds. \qquad (11)$$

Where, t is the thickness of the element.

By applying Castigliano's theorem to eq.(11) the following stiffness equation can be derived:

$$\frac{\partial V}{\partial u} = \boldsymbol{K}.\boldsymbol{u} = \boldsymbol{F} \qquad (12)$$

Where K is the stiffness matrix and F is the centroidal load. F is defined by the following equation:

$$\boldsymbol{F} = \left[X_1, Y_1, M_1; X_2, Y_2, M_2\right]^T \qquad (13)$$

3.2. Model of Pr-bar [2), 3)]

The pr-bars were introduced into the RBSM using the beam element model, which considers the deformation of two bars connected by a system spring as shown in figure 6.

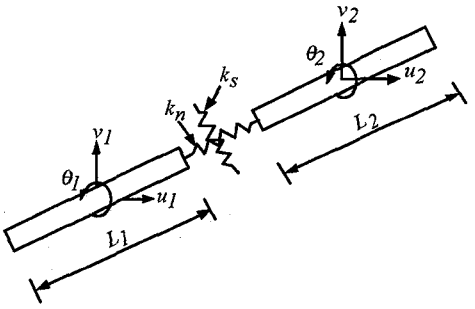

Figure 6 Beam Element Model

Using the same process described in section 3.1, the expression of k_n and k_s can be derived as follows:

$$k_n = \frac{2E}{(L_1+L_2)}$$
$$k_s = \frac{E}{(1+\nu)(L_1+L_2)} \qquad (14a, 14b)$$

The strain energy stored in the spring system is given by the following equation.

$$V = \frac{1}{2}u_i^T \int_A \left(\boldsymbol{B}^T.\boldsymbol{D}.\boldsymbol{B}\right)dA.\boldsymbol{u_i} \qquad (15)$$

Where, A is the cross-section area of the bar element.

Figure 7 shows the model proposed in this analysis, taking the spring constant k_s=0.

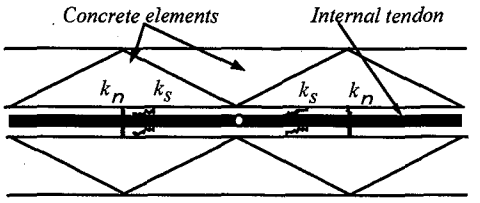

Figure 7 Assumed Model for Pr-Bar

3.3. Model of SFRC

The SFRC and plain concrete have almost the same stress-strain relation in compression area even after strain softening point. However, in the tension area, the SFRC has a different stress-strain relation that dominates the behavior of the structure after crack occurrence. Introducing the SFRC into the RBSM, the tensile stress-strain relationship of the plain concrete shown in figure 3 was modified as shown in zone II and III of figure 8, $f_r' = 0.83 f_t'$ and $\alpha_1 = 0.053 f_t'$ [4]. In this analysis, the total strain-softening behavior was adopted as an execution of n times repeats of release stress, σ_{cn}, as shown by the dashed line in figure 9.

3.4. Nonlinear Analysis Algorithm and Element Mesh

The analysis was carried out according to an incremental displacement method. Figure 10 shows the algorithm proposed for material nonlinear analysis [8], in which R_{min} method was modified to add the released force to the remaining load while counting the applied load, and to take into account the cracking and compressive failure.

The exact value of the spring constant k_n used in the joint was determined from the stress-strain relation of a compression test (E=5.4 GPa).

The element mesh used in this analysis is shown in figure 11, where the non-smudgy element indicates the concrete and the steel reinforced concrete elements, the smudgy element corresponds to SFRC element. The thick line shows the pr-bar. Particular triangular elements, shown as line element, were used for the support point, loading point and laterally immovable plane at mid-span. A total of 218 nodes and 272 elements were used.

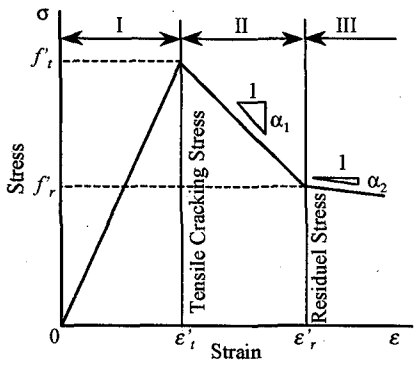

Figure 8 Tensile Stress-Strain Relationship of SFRC

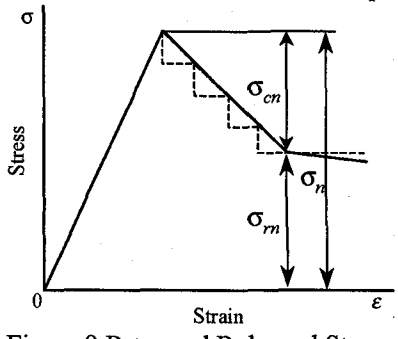

Figure 9 Proposed Released Stress

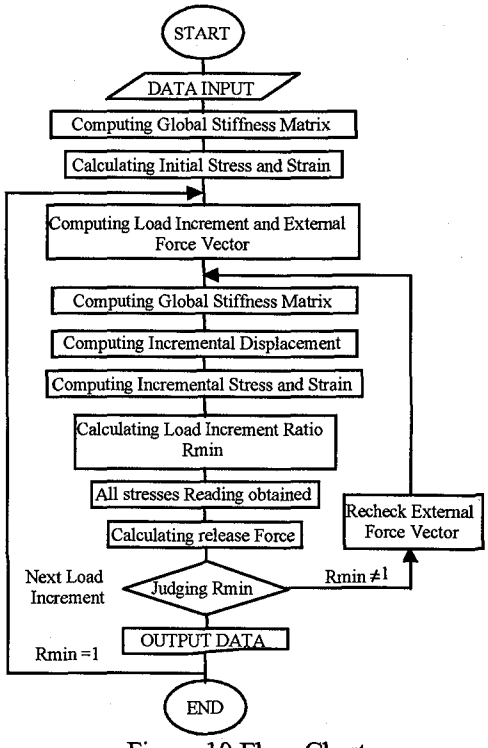

Figure 10 Flow Chart

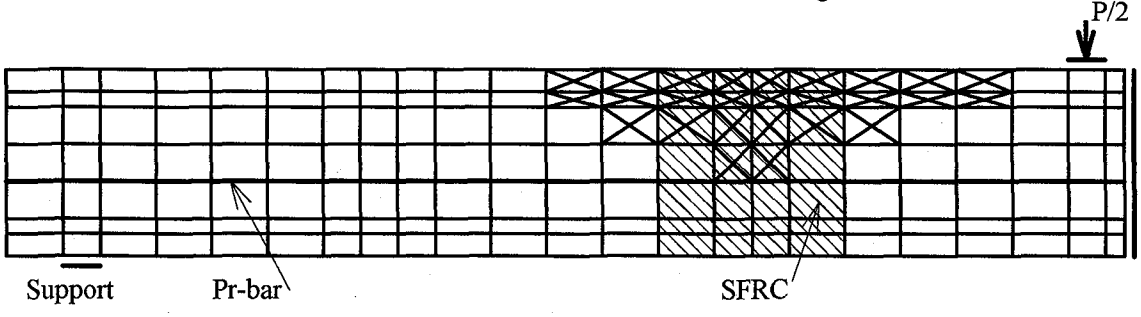

Figure 11 Mesh Division for Half Part of Specimen

4. RESULTS AND DISCUSSION

4.1. Displacement Behavior

Figure 12 shows the experimental and analytical load vs. the deflection at mid-span for the two cases. In the experimental results, there is an obvious difference in the deflection behavior of case 1 and case 2. In addition, a large displacement and an increase of the carrying load was observed in case 2. It is considered directly due to the effect of the steel fiber mixed to the concrete in the end-side of the precast elements. It can also be observed that the analytical results are in good agreement with the experimental ones, except the failure load for case 1, where the experimental value was lower than the analytical one due to sudden failure in experiment.

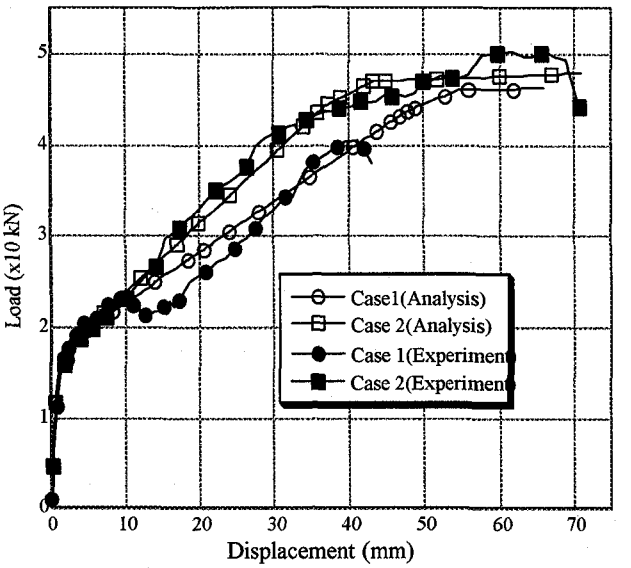

Figure 12 Load-Displacement Behavior

4.2. Strain Behavior

a- Strain in pr-bar

Figure 13 shows the load-strain relation in the pr-bar. In two cases, almost the same behavior was observed. It is remarkably clear that the analytical results fitted with the experimental results.

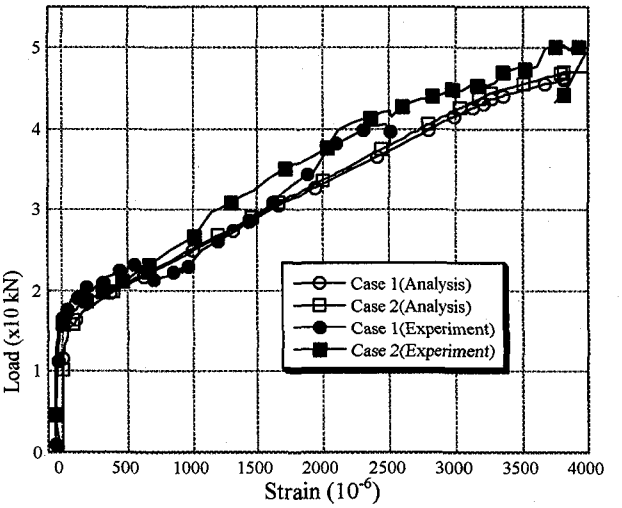

Figure 13 Load-Strain Behavior in Pr-bar

b- Compression strain in concrete

Figure 14 shows the load-compressive strain behavior on the upper side of the joint. The relationship between the applied load and the compressive strain changes proportionally up to the failure of the structure. These results were approved by the analysis.

c- Tension strain in concrete

Figure 15 shows the load-tensile strain behavior on the bottom side of the joint. Up to the opening of the joints, the relationship between the applied load and concrete strain changes proportionally. However, in the stage exceeding the opening of the joints, it is observed that the strains do not increase. These results were approved by the analysis.

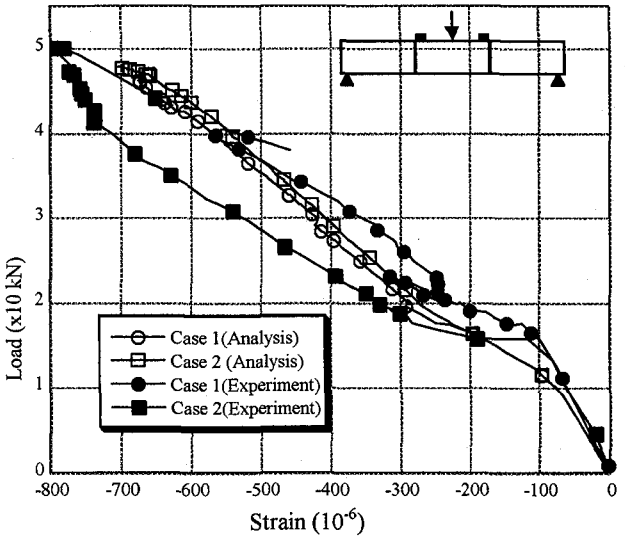

Figure 14 Load-Compressive Strain Behavior

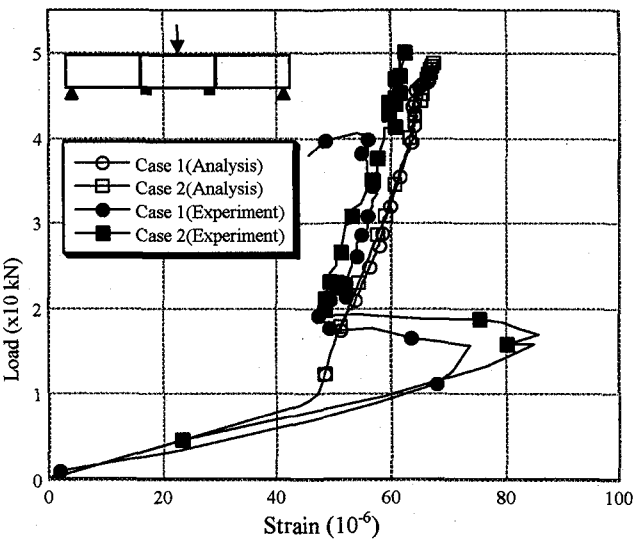

Figure 15 Load-Tensile Strain Behavior

4.3. Joint Opening Behavior

The behavior of the joint opening vs. the applied load is shown in figure 16. Up to the opening of the joints, the relationship between the applied load and the joint's opening changes proportionally. However, after a certain value of the joint's opening, slip between the concrete elements was observed. Therefore, it becomes difficult to get the exact opening from the experiment.

On the other hand, the analytical results are well fitted with the experimental ones up to the beginning of the slip between blocks.

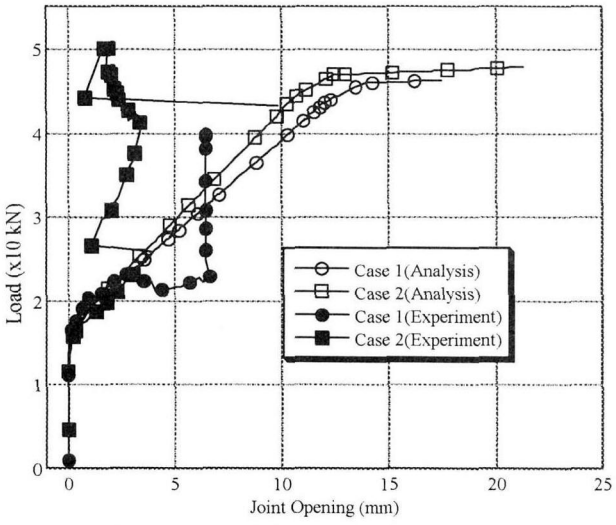

Figure 16 LoJoint Opening (mm) Behavior

4.4. Failure Mode

Photo 1 and photo 2 show the crack pattern observed during the experiments of, respectively, case 1 and case 2. In the two cases, the first cracks were flexural cracks in the central element of the structure. After the opening of the joints, shear cracks were observed in the upper side of the central element.

For the structure without SFRC (case 1), the shear cracks propagate up to the center of the element. However, in case 2, the use of steel fiber limits the propagation of the cracks. Figure 17 shows the pattern obtained from the RBSM analysis, it can be observed that the crack pattern is very similar to the experimental one.

Photo 3 and photo 4 show two completely different failure modes. In case 1, a sudden failure due to crash of the upper side of the concrete was observed. In case 2, the structure resists much more than case 1 and the failure was due to compression in the upper side of the joints.

5. CONCLUSION

In this study, we have investigated the partial use of SFRC in a precast structure, and the application of the RBSM to analyze the behavior of a precast beam with SFRC. The results obtained are summarized as follows:

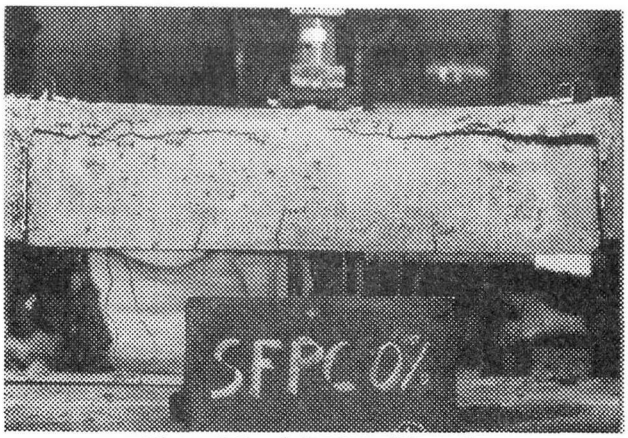

Photo 1Crack Pattern (Case 1)

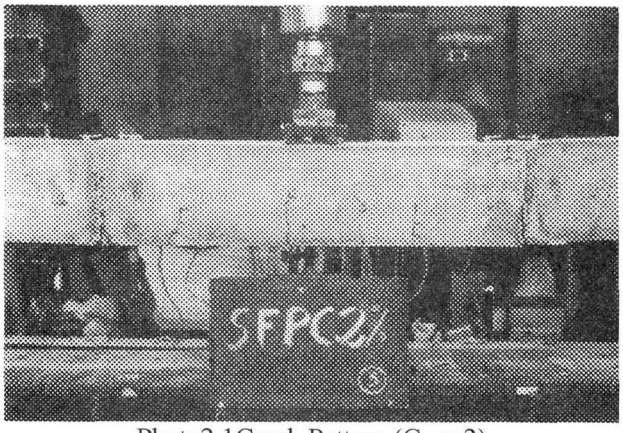

Photo2 1Crack Pattern (Case 2)

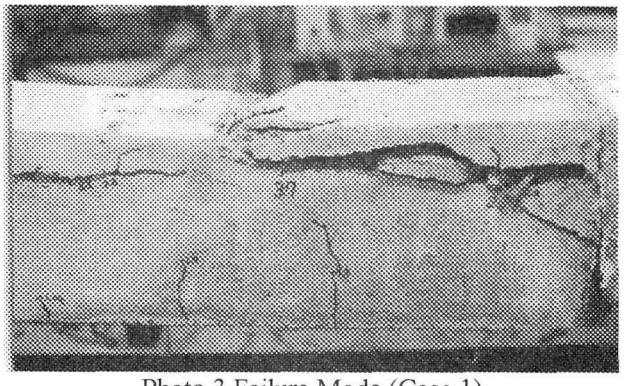

Photo 3 Failure Mode (Case 1)

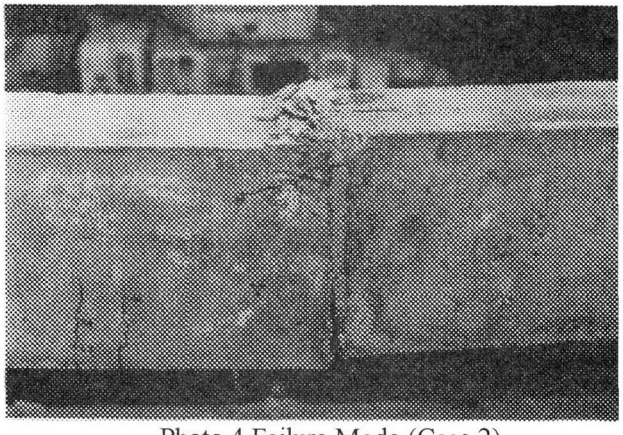

Photo 4 Failure Mode (Case 2)

1. Using SFRC in the joint part of a precast structure can increase the serviceability, restrain the crack propagation, and prevent a sudden failure of the structure.
2. A partial use of SFRC instead of a full use of SFRC in a precast structure is sufficient to reinforce the structure and to reduce the cost.
3. The rigid bodies-spring model incorporating the stress-strain model proposed for the SFRC and the proposed model for the prestressing tendons is an effective method to analyze the behavior of a precast structure containing steel fiber.

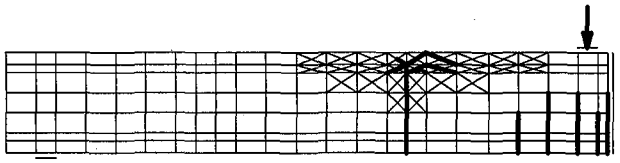

Case 1

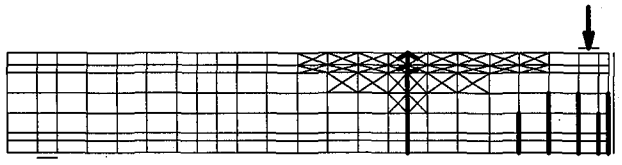

Case 2

Figure 17 Crack Pattern

References

1) Kawai, T., New Element Models in Discrete Structural Analysis, Journal of the Society of Naval Architects of Japan, No.141, pp. 174-180, 1977.
2) Zardoum, H. et al., Application of Rigid Bodies Spring Model to Precast Members Prestressed With Internal and External Tendons, Journal of Structural Engineering, JSCE, Vol. 44A, pp. 359-366, 1998.
3) Kawai, T. and Chen, C.N., Discrete Element Analysis of Beam Bending Problems Including the Effect of Shear, Seisan-Kenkyu, Monthly Journal of Institute of Industrial Science, Vol. 30, No. 4, pp. 165-168, 1978.
4) Zardoum, H. et al., An Analysis of Flexural Behaviour on Steel Fibre Reinforced Concrete Beam, Proceeding Of the Asia-Pacific Specialty Conference on Fibre Reinforced Concrete, pp. 277-284, Singapore, 28-29 August 1997.
5) Bantia, N., Fiber Reinforced Concrete: Present and the Future, Proceeding of the Asia-Pacific Specialty Conference on Fibre Reinforced Concrete, pp. 1-10, Singapore, 28-29 August 1997.
6) Bentur, A., Fiber-Reinforced Cementitious Materials, Material Science of Concrete I, Jan P., Skalny, pp. 223-284, 1989.
7) Kitoh, H., Takeuchi, N., et al., Size Effect Analysis of Plain Concrete Beam by Using RBSM, Proceeding of the Second International Conference on Analysis of Discontinuous Deformation, pp. 373-382, Kyoto, Japan, 1997.
8) Ueda, M., Takeuchi, N., et al., Discrete Limit Analysis of Reinforced Concrete Structures Including the Effects of Tensile and Compressive Failure, Journal of Structural Engineering, JSCE, Vol. 36A, pp. 315-323, 1990.

(Received September 18, 1998)